Angular Reflectance of Leaves With a Dual-Wavelength Terrestrial Lidar and Its Implications for Leaf-Bark Separation and Leaf Moisture Estimation

Steven Hancock, Rachel Gaulton, and F. Mark Danson

***Abstract*— A new generation of multiwavelength lidars offers the potential to measure the structure and biochemistry of vegetation simultaneously, using range resolved spectral indices to overcome the confounding effects in passive optical measurements. However, the reflectance of leaves depends on the angle of incidence, and if this dependence varies between wavelengths, the resulting spectral indices will also vary with the angle of incidence, complicating their use in separating structural and biochemical effects in vegetation canopies. The Salford Advanced Laser Canopy Analyser (SALCA) dual-wavelength terrestrial laser scanner was used to measure the angular dependence of reflectance for a range of leaves at the wavelengths used by the new generation of multiwavelength lidars, 1063 and 1545 nm, as used by SALCA, DWEL, and the Optech Titan. The influence of the angle of incidence on the normalized difference index (NDI) of these wavelengths was also assessed. The reflectance at both wavelengths depended on the angle of incidence and could be well modelled as a cosine. The change in the NDI with the leaf angle of incidence was small compared with the observed difference in the NDI between fresh and dry leaves and between leaf and bark. Therefore, it is concluded that angular effects will not significantly impact leaf moisture retrievals or prevent leaf/bark separation for the wavelengths used in the new generation of 1063- and 1545-nm multiwavelength lidars.**

***Index Terms*— Laser radar, remote sensing, technology assessment, vegetation.**

I. Introduction

TERRESTRIAL vegetation plays a key role in many processes, and knowledge of its structure and biochemistry is needed to understand its function. Data from passive optical sensors are widely used to map and monitor vegetation, but are unable to separate structural and biochemical effects [1], requiring either direct measurements (limited in coverage) or assumptions of either structure or biochemistry to study vegetation processes. Lidar's ability to measure vegetation structure has been comprehensively proven in a large number of studies [2]–[4].

A new generation of terrestrial and airborne multiwavelength lidars has the potential to simultaneously measure structure and biochemistry by making measurements of range and reflectance of multiple wavelengths at high resolution (hemispherical scans of 1-mrad spacing for terrestrial and up to 80 points/m^2 for airborne). This allows improved land cover classifications [5], [6] and vegetation biochemistry to be studied [7], [8]. Terrestrial laser scanner (TLS) systems have been tested in laboratory conditions on individual leaves at fixed angles of incidence to show that leaf water [8] and chlorophyll content [9] can be derived. In field conditions, leaves will be at a range of angles of incidence, and previous studies have shown that leaf reflectance depends on the angle of incidence [10]–[12]; therefore, the estimates of biochemistry could depend upon the angle of incidence. For example, Eitel *et al.* [13] found that for their dual-wavelength lidar (532 and 658 nm), angular effects limited the accuracy of leaf nitrogen estimates. Kaasalainen *et al.* [14] tested three spectral indices using an eight wavelength lidar (between 555 and 1000 nm) and found that differences in angular reflectances between the visible and infrared wavelengths caused large angular dependencies. However, the results of Shi *et al.* [15] contradict both of these studies, finding no angular dependence of three spectral indices using wavelengths between 556 and 780 nm, and so there is some uncertainty in the literature.

The reflection of light from, or penetration through, a leaf surface and absorption by elements within a leaf depend on the wavelength, particularly the ratio of the wavelength to scatterer size. At near infrared (NIR), light is only absorbed by the relatively sparse leaf dry matter and so there may be significant multiple scattering within the leaf, whilst at shortwave infrared (SWIR), absorption is dominated by water and so the amount of within-leaf multiple scattering may depend on water content [16]. At visible wavelengths, chlorophyll absorbs most of the light that penetrates into a leaf, and so the majority of reflected light is from the leaf surface [14].

Manuscript received June 27, 2016; revised December 3, 2016; accepted December 30, 2016. Date of publication March 15, 2017; date of current version May 19, 2017. The work of R. Gaulton and S. Hancock was supported by the NERC New Investigators under grant NE/K000071/1, with additional funding from the Douglas Bomford Trust.

S. Hancock is with the Department of Geographical Sciences, University of Maryland at College Park, College Park, MD 20742 USA (e-mail: svenhancock@gmail.com).

R. Gaulton is with the School of Civil Engineering and Geosciences, Newcastle University, Newcastle upon Tyne NE1 7RU, U.K.

F. M. Danson is with the School of Environment and Life Sciences, University of Salford, Salford M5 4WT, U.K.

Color versions of one or more of the figures in this paper are available online at http://ieeexplore.ieee.org.

Digital Object Identifier 10.1109/TGRS.2017.2652140

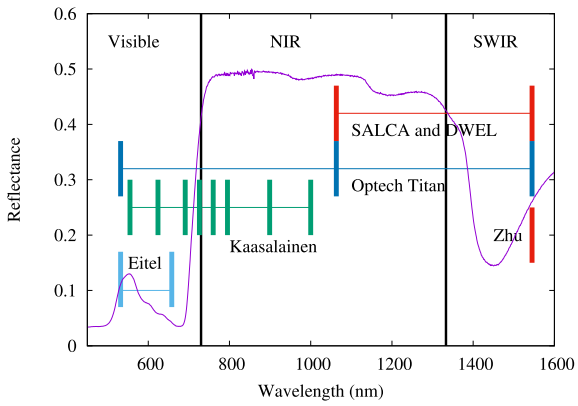

Fig. 1. Leaf reflectance with optical regimes labeled and wavelengths of SALCA, DWEL, and Optech Titan and those of instruments used in the previous studies of Kaasalainen *et al.* [14], Eitel *et al.* [13], and Zhu *et al.* [12].

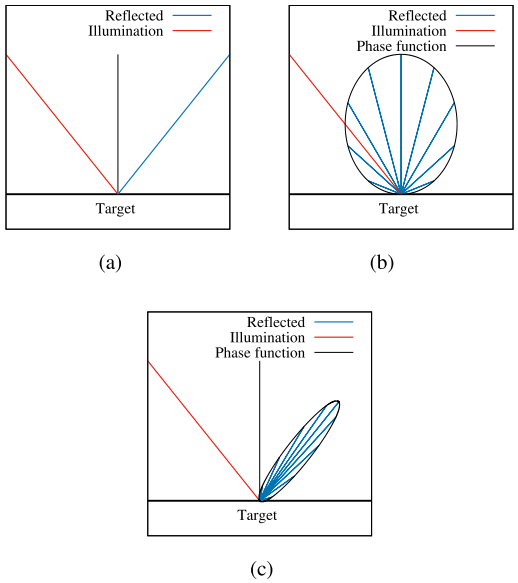

Fig. 2. Illustration of phase functions. The length of reflected ray lines indicates relative intensity, and the phase function envelope (black curve) shows the intensity returned at all angles. The integral of the phase function envelope is the single scattering albedo for targets with no transmittance. (a) Specular. (b) Lambertian. (c) Mixed.

These three optical regimes of leaves are shown in Fig. 1 along with the wavelengths of this and previous studies.

The reflectance as a function of the angle of incidence of the detector, called the phase function, depends upon the above-mentioned scattering mechanisms and the angle of incidence of targets within the illuminated footprint. The two extreme phase functions are specular reflection [Fig. 2(a)], where energy is reflected in a single direction, like a mirror, and Lambertian reflection [Fig. 2(b)], where energy is scattered in all directions with the relative intensity of scattered rays equal to the cosine of the angle of incidence of the emitted light [17]. Reflections can also be combinations of the two [Fig. 2(c)]. For lidar measurements of leaves, wavelengths that penetrate into the leaf will experience multiple scattering, so are likely to have a near-Lambertian phase function [Fig. 2(b)]. Reflections from wavelengths that are strongly absorbed within the leaf will be made up of mainly surface reflections, which are predominantly specular [Fig. 2(a)], although roughness within the laser footprint spreads this out to be more like Fig. 2(c), and so the relative size of the laser footprint to the target roughness is also important. A 5-mm TLS spot is likely to illuminate a single, smooth target, whilst a 20-cm airborne lidar footprint may illuminate multiple objects, increasing the roughness. Note that lidars measure in the hot-spot direction [18], where the light source and detector view along the same vector, and so they do not experience the same bidirectional reflectance effects due to macrostructure as passive systems [17], only target scattering mechanisms [19].

A lidar illuminating a specular target will receive little return energy unless the laser is at right angles to the surface. A lidar illuminating a Lambertian target will receive energy proportional to the cosine of the angle of incidence [30]. The ratio of specular to Lambertian reflectance from a leaf is then controlled by the ratio of light returned from multiple scattering within the leaf and single scattered light from the surface (in turn controlled by the within leaf absorption at that wavelength) and the variation in the angles of incidence within the laser footprint (controlled by laser footprint size and surface roughness).

The angle of incidence will never be known for all targets in a vegetation canopy, especially for small leaves and needles, and so in order to use spectral indices in the field, the phase functions at the two wavelengths must be near constant. The majority of past studies have used passive systems. The particular arrangement and coherence of lidars could significantly deviate from these measurements [17], [18] and the angular dependence of spectral indices from the wavelengths used by the new generation of dual-wavelength lidars (1063 and 1545 nm) have not yet been investigated.

This paper investigates whether the wavelengths used in the two currently operational dual-wavelength, full-waveform TLS instruments, Salford Advanced Laser Canopy Analyser (SALCA), and DWEL (Dual-Wavelength Echidna Lidar) [20], [21], have significantly different phase functions and so will cause the derived spectral indices, such as the normalized difference index (NDI) [see (1)] to vary. The magnitude of any variation in the NDI was compared with the change in the NDI with leaf moisture and between leaves and bark, which are the distinctions that the SALCA lidar is designed to make [8], [20]. These wavelengths are also used in the multiband Optech Titan airborne lidar [5] and combinations of Riegl airborne systems [22] and so the results have relevance beyond TLS, although the larger laser footprint of airborne sensors compared with TLS will mean that a range of angles of incidence will always be encountered. In addition, the Riegl VZ-400 TLS has a single 1545-nm laser and the intensity of returns has been used to separate leaf and bark [4], [23] and to measure leaf moisture when the angle of incidence is known [12], and so it is important to understand the dependence of intensity on the angle of incidence.

II. Materials and Methods

A. Lidar

Data were collected using the SALCA dual-wavelength, full-waveform TLS [20]. The return energy was calculated using the "sum method" described by Hancock *et al.* [24]

found to be the most accurate for SALCA. This was calibrated to reflectance using nonlinear fitting to returns from targets of known reflectance, described in Appendix A. The NDI accuracy was 0.055 root-mean-square error (RMSE) with a bias of 0.027. Scans were performed at 1-mrad resolution, giving a point spacing of 6 mm and laser footprints of 9 mm for 1063 nm and 10 mm for 1545 nm at the leaf samples 6 m from the scan center. This gave a 9–10-mm resolution image of the target at 1063 and 1545 nm.

The NDI of the two reflectances, given by the following equation, was calculated for each laser shot:

$$\mathrm{NDI} = \frac{\rho_{1063} - \rho_{1545}}{\rho_{1063} + \rho_{1545}} \tag{1}$$

where ρ_{1063} and ρ_{1545} are the reflectances at 1063 and 1545 nm, respectively. The mean reflectances and NDIs were calculated for each leaf, only including laser shots that were entirely blocked by leaves.

B. Leaves

Leaves were collected from complete plants at the Newcastle University Botanic Gardens during March 2013. Due to the time of year, the choice was limited to evergreen and indoor plants. Eucalyptus (species unknown) was chosen to represent matt leaves and peace lily (*Spathiphyllum*) and laurel (*Laurus nobilis*) to represent glossy leaves. Fresh and browning eucalyptus leaves were used to assess the impact of leaf health on phase function. Measurements were taken of three brown eucalyptus leaves, seven fresh eucalyptus (alternating topside and underside), one peace lily, and one laurel. Measurements of leaf water content were not made due to time constraints.

Leaves were suspended in a frame by thin black thread, shown in Fig. 3. Note that the dark lines around objects are due to partial hits [25], which were not used in the analysis. This thread covered only a small area of leaf and so had a negligible effect on the total leaf reflectance. The frame was mounted on a tripod with a built in protractor. The whole frame was rotated and separate scans made in 5° increments from −50° to +50° (at angles of incidence greater than 50°, the leaf signal became mixed with returns from the leaf holder and so could not be used). This gave two repeat measurements per laser angle of incidence. For some leaves, the angular range was smaller due to their position in the holder. Absolute leaf angle accuracy was on the order of 10° (due to leaves not lying flat to the frame) and relative accuracy was around 1° (finer steps could not accurately be seen on the tripod protractor). The frame was 42 cm across so that leaves at the extremes would have slightly different angles of incidence. The variation in the leaf angle was accounted for by calculating the angle of maximum reflectance (normal angle of incidence) separately for each leaf.

C. Angular Reflectance

The angular dependence of reflectance was quantified by fitting a cosine function to the observed reflectance with angle [11]

$$y = A_y \cos(2(\theta - \mu)) + \nu \tag{2}$$

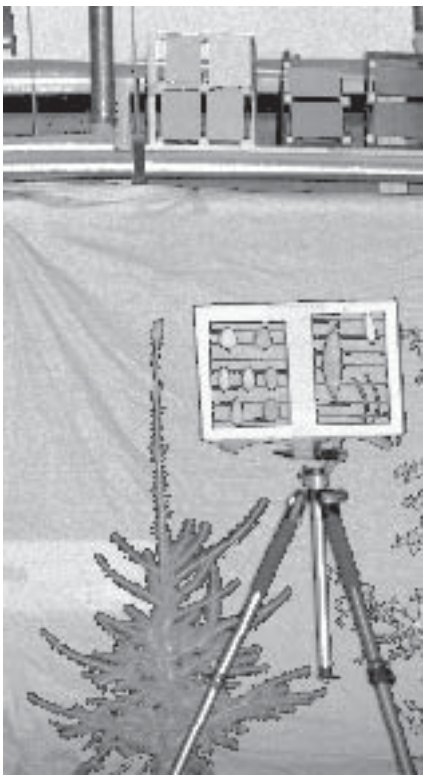

Fig. 3. SALCA scan of the leaf holder on rotatable tripod with calibration panels above. Other objects in the scene were for different experiments.

where A is the amplitude, describing the magnitude of the angular dependence, θ is the angle of incidence, μ is the angle of the peak reflectance, which will be the leaf holder angle at which that leaf was normal to the laser, and ν is an offset to allow the NDI to have a nonzero base (the NDI will not be zero at an angle of incidence of 90°). y can either be the reflectance at 1545 or 1063 nm (ρ_{1545} or ρ_{1063}, respectively) or the NDI.

D. Nonangular NDI Variations

In order to assess the impact of any NDI variation with the angle of incidence on a dual-wavelength lidar's ability to distinguish leaf from bark [20] or to estimate leaf water content [8], the magnitude of NDI variations due to these factor was assessed and compared with the variations due to the angle of incidence.

To assess the change in the NDI with leaf water, leaves from eucalyptus (four leaves), calico flower, *Aristolochia elegens* (two leaves), avocado pear tree (*Persea americana*, two leaves), bird's nest fern, *Asplenium nidus* (two leaves) and jade plant, *Crassula ovata* (three leaves), collected from the former Newcastle University botanic gardens, were measured by an ASD Field Spec Pro spectroradiometer with a contact probe (ASD inc., Boulder, CO, USA), scanned by SALCA and weighed at regular intervals as they dried in air. These were different leaves to those used in the angular reflectance experiments. The leaves started at complete health and were allowed to dry naturally over two days, with repeat measurements taken as often as possible (every 2–3 h during the day). The ASD contact probe had a 1-cm window, provided

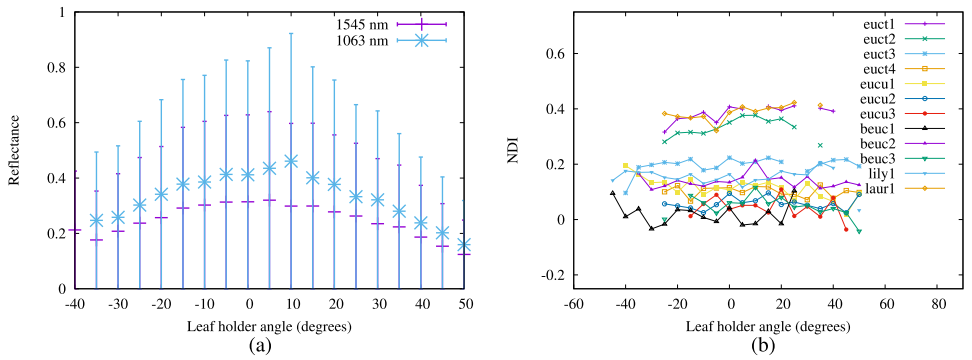

Fig. 4. Reflectance against leaf holder angle for one representative leaf and NDI against leaf holder angle for all leaves. Note that leaves may not have been aligned with the leaf holder. Bars show one standard deviation of reflectance between SALCA footprints. (a) Reflectance, brown eucalyptus, beuc1. (b) NDI.

its own illumination source and maintained a constant view geometry (detector fixed at 8° to target), ensuring that angular and structural effects were constant between measurements. The SALCA measurements were not used in this paper, instead the ASD-measured spectra were used to calculate the NDI at the same wavelengths as SALCA, which gave the same trend as the SALCA data but with less noise. Leaf water content was calculated by dividing leaf weights by the dry weight, found by weighing after placing in an oven at 40 °C for three days. This is a repeat of the experiment described by Gaulton *et al.* [8].

To assess the difference between leaf and bark NDI, spectra from a range of leaf and bark samples from the LOPEX93 database [26] were examined. This included leaf and bark reflectance measured by a Perkin Elmer Lambda 19 double-beam spectrophotometer with a BaSo4 integrating sphere, which measures the integrated hemispheric reflectance. The NDI at SALCA's wavelengths from all leaves (315 spectra covering a wide range of species) and bark (five spectra) samples in the database were extracted and the separation of the means and overlap of the resulting distributions calculated. Only a very small number of bark samples were available and these results can only be considered as tentative.

III. Results

Fig. 4(a) shows the reflectance against leaf holder angle for a single leaf (a brown eucalyptus), which has a similar shape to all other leaves. Bars on the reflectance plot show one standard deviation between SALCA footprints across the leaf (each footprint gave one measure of reflectance). These are larger than the between-angle variation due to instrument noise and variation within a leaf, especially along veins [8]. Noise contributed up to a maximum of 5.5% of the variation, from the calibration assessment in Appendix C. Reflectance for all leaves showed a clear cosine angular dependence. Only two out of three of the brown eucalyptus leaves (beuc2 and beuc3) showed a small specular peak for 1063 nm and so the NDI. This is likely to be due to the lack of multiple scattering within the brown leaf so that specular reflection from the surface was relatively stronger than for the healthy leaves [11]. None of the fresh leaves showed this specular effect, including the waxy laurel and peace lily leaves. Whilst these leaves do have strong specular peaks at visible wavelengths, this was not apparent from these measurements made in the infra-red, most likely due to within-leaf scattering.

TABLE I

Amplitude of Fitted Angular Function (2) for SALCA Measured Reflectance at Each Wavelength ($A_{\rho 1545}$ and $A_{\rho 1063}$) and NDI (A_{NDI}) Along With the Mean NDI ($\overline{NDI}$)

Leaf	A_{NDI}	$A_{\rho 1545}$	$A_{\rho 1063}$	$\overline{NDI}$	Label
Eucalyptus underside	0.036	0.144	0.201	0.11	eucu1
Eucalyptus underside	0.022	0.215	0.241	0.06	eucu2
Eucalyptus underside	0.013	0.231	0.234	0.05	eucu3
Eucalyptus topside	0.022	0.025	0.220	0.20	euct1
Eucalyptus topside	-0.005	0.213	0.319	0.10	euct2
Eucalyptus topside	0.058	0.067	0.258	0.38	euct3
Eucalyptus topside	0.140	0.054	0.245	0.33	euct4
Brown eucalyptus	0.005	0.322	0.396	0.04	beuc1
Brown eucalyptus	0.024	0.161	0.227	0.14	beuc2
Brown eucalyptus	0.080	0.260	0.412	0.05	beuc3
Peace lily	-0.004	0.096	0.144	0.15	lily1
Laurel	0.038	0.088	0.375	0.39	laur1

The angular dependence of reflectance should be taken into account when attempting to calculate partial hit area for gap fraction [25] and may need to be accounted for when using a single wavelength lidar to separate leaf from bark [4], [23] or to estimate biochemistry, which in turn requires knowledge of the angle of incidence of the target [12]. It should be noted that the leaf from bark separation used by Béland *et al.* [23] and Calders *et al.* [4] relied upon leaves having a lower reflectance than bark at 1545 nm, and so, these leaf angular effects would help rather than hinder the distinction, although the change in bark reflectance with the angle of incidence was not measured, which may impact the separability. Measuring biochemistry from single wavelength lidar may be more problematic as the angle of incidence must be known for every return [12], which will be a considerable challenge.

Fig. 4(b) shows the NDI against the angle of incidence for all leaves. The amplitudes of the cosines fitted to describe the variation of the NDI and reflectance with the angle of incidence [A in (2)] are shown in Table I, along with the mean NDI for all footprints within each leaf. The mean of the angular NDI amplitude for all leaves (mean of A_{NDI}) was 0.026, which is less than the noise level. There was a single outlier for the fresh eucalyptus leaves (euct4) with an NDI amplitude of 0.14. This was due to a specular peak in

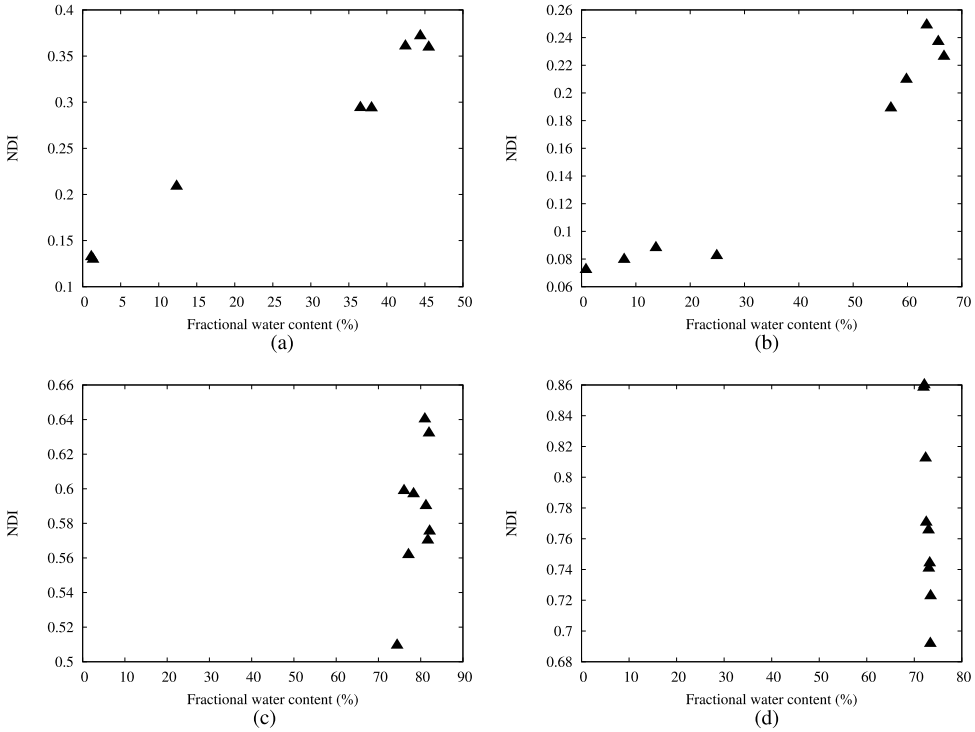

Fig. 5. ASD measured NDI against leaf weight whilst drying for two broadleaves and two succulent leaves. (a) Eucalyptus, euc1. (b) Avocado pear tree, avc1. (c) Bird's nest fern, fer1. (d) *Jade plant, jad1*.

TABLE II
TOTAL CHANGE IN FRACTIONAL LEAF WATER CONTENT (Δw) AND ASD MEASURED NDI (ΔNDI) FOR LEAVES DRYING IN AIR OVER TWO DAYS

Leaf	Δw	ΔNDI	Label
Calico flower	66.2 %	0.20	cal1
Calico flower	64.2 %	0.35	cal2
Eucalyptus	46.8 %	0.23	euc1
Eucalyptus	45.8 %	0.22	euc2
Eucalyptus	46.8 %	0.17	euc3
Eucalyptus	43.9 %	0.23	euc4
Avocado pear	65.9 %	0.15	avc1
Avocado pear	69.0 %	0.14	avc2
Bird's nest fern	7.7 %	0.07	fer1
Bird's nest fern	17.1 %	0.08	fer2
Jade plant	1.5 %	-0.14	jad1
Jade plant	1.0 %	0.01	jad2
Jade plant	1.0 %	0.02	jad3

the 1063-nm reflectance and may have been exacerbated by a smaller angular range ($-25°$ to $25°$) for that leaf due to its position in the holding frame, increasing the uncertainty of the cosine fitting. In all cases, reflectance at 1063 nm showed a greater angular dependence than that at 1545 nm, but the normalized difference of the two reflectances varied less than the instrument noise, except for the single outlier. The specular peaks for brown eucalyptus leaves at 1063 nm caused a peak in the NDI 0.06 higher than the mean, a small amount, comparable to instrument noise.

A. Results for Nonangular NDI Variations

Table II shows the total change in leaf water content (fraction of leaf weight made from water) and ASD measured NDI for the drying leaves. Fig. 5 shows some representative examples. The eucalyptus, calico flower, and avocado pear

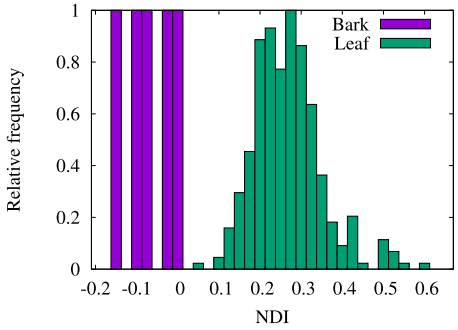

Fig. 6. NDI histograms for leaf and bark from the LOPEX93 database.

tree leaves showed a mean change in the NDI of 0.2 as the leaf water content reduced by 50%. The succulent leaves (jade plant and bird's nest fern) had much smaller decreases in leaf water content and much smaller corresponding NDI increases. For the leaves that did show a significant change in water content, the change in the NDI during drying was a factor of 10 greater than the angular NDI amplitudes found (which were smaller than the noise level). Gaulton *et al.* [8] showed NDI varying by 0.4 across the observed range of leaf water content, larger than the magnitude found here, although this included the difference between leaves of different thicknesses and so starting leaf water contents. For the nonsucculent leaves tested, an angular uncertainty in the NDI of 0.02 would give a minimum detectable water content change of 0.9%, whilst the noise limit of 0.055 would set the minimum detectable water content change to 2.4%.

Histograms of the NDIs of the leaf and bark samples in the LOPEX93 database [26] are shown in Fig. 6. They had a mean difference of 0.34 and there were no leaves with

NDIs within 0.026 (the mean angular amplitude) of the highest bark NDI. Therefore, the variation in leaf NDI due to angular effects is small compared with the difference between leaf and bark NDI for the small number of bark samples tested. The change in the NDI with the angle of incidence of bark was not measured as this paper's primary focus was on detecting leaf moisture. These results can only be considered to be tentative. However, as all wavelengths will scatter from the surface as opposed to different regimes interacting differently (Fig. 1), it is hypothesized that bark NDI should show less angular dependence than leaves.

IV. Conclusion

It is concluded that whilst reflectance of vegetation at the wavelengths used by the new generation of multiwavelength lidars (1063 nm in the NIR and 1545 nm in the SWIR) showed angular effects, the impact of this on the NDI was small, smaller than the uncertainty from instrument noise. The change in the NDI with leaf water content was larger than the change with the angle of incidence. Brown (unhealthy) leaves showed greater dependence of the NDI on the angle of incidence than fresh leaves, but the maximum observed NDI amplitude was smaller than the change with moisture content and comparable to the noise limit. This angular effect may set a lower limit on the detectable moisture content change. Therefore, the NDI can be used to investigate leaf water content [8] without the knowledge of the angle of incidence of the target, greatly simplifying the application of TLS to canopy scale moisture estimates [12]. These wavelengths, 1063 and 1545 nm, do not suffer from the difference in angular reflectance for leaves between near infra-red and visible lasers reported in previous studies [13], [14] due to the different optical regimes.

Similarly, the difference between leaf and bark NDI values were large compared with the variation of leaf NDI with the angle of incidence, and so, we tentatively conclude that angular effects are unlikely to have an impact on the ability of dual-wavelength TLS to separate leaf and wood, although a very small sample of bark samples were available. The change in the NDI with the bark angle of incidence was not investigated, and further work in this area is ongoing.

Appendix

A. Calibration Equation

The method proposed to calibrate SALCA by Schofield *et al.* [27] could not be implemented here as the laser temperature sensors required for that method had not been installed when this study was performed. An alternative method was developed, using targets of known reflectance to calculate laser power.

For SALCA, the recorded digital number DN is nonlinearly related to the effective target reflectance ρ_{eff} observed to be

$$\text{DN} = (m\rho_{\text{eff}} + c)(1 - e^{-k\rho_{\text{eff}}}) \tag{3}$$

where m, c, and k are fitting constants, and ρ_{eff} is the effective reflectance of the target, given by

$$\rho_{\text{eff}} = \rho \Psi P_0 f(r) \frac{A_p}{A_f} \tag{4}$$

where ρ is the target reflectance, Ψ is the angular phase function, P_0 is the outgoing laser power as a fraction of the maximum, $f(r)$ is the range dependence function, and A_p/A_f is the ratio of the projected area of the target A_p to the footprint area A_f. For a target that fully fills the field of view $A_p/A_f = 1$. The laser power P_0 varies from scan to scan and is a function of laser temperature. ρ of each target was measured using an ASD Field Spec Pro spectroradiometer with contact probe (ASD inc., Boulder, CO, USA), and Ψ was set to one as the calibration panels were fixed near orthogonal to the laser beam throughout the experiment.

By plotting the reflectance against the range for scans that were known to have constant laser power (scans for which the fixed range targets had consistent return strengths), the range dependence was found to be

$$f(r) = \frac{1}{r^a}(1 - e^{-k_2 r^{k_3}}) \tag{5}$$

where r is range, and a, k_2, and k_3 are fitting constants. This is similar to the calibration method developed for DWEL [30].

B. Calibration Data

Two calibration panels were used, each with six targets of known reflectance [measured with an ASD Field Spec Pro spectroradiometer with contact probe (ASD inc., Boulder, CO, USA)] using a water-based matt paint (J. Armston, 2013, Personal Communication). Barium sulphate powder was added to the brightest panel to reduce specular reflection. One panel was fixed at a range of 8 m, whilst the second was varied between 2 and 60 m from SALCA's scan center. Scans were made at different ranges, taking care to cover the ranges of known features in (5).

C. Fitting the Calibration

The calibration parameters were determined by fitting the observed DN to the known ρ_{eff} values of the calibration panels using the MINPACK implementation of the Levenberg–Marquardt method [29]. Initially, an attempt was made to fit all parameters to all the data at the same time, but strong coupling between variables, particularly m and P_0, prevented an accurate result. Instead, first the nonlinear response variables (m, c and k) were found by fitting (3) to the single scan of the fixed range (8 m) target that best straddled an observed nonlinearity at a DN of 350, so that P_0 and $f(r)$ could be treated as constants of 1.

Next the laser powers P_0 were found for each scan by fitting (3) and (4) to the fixed range targets using the known values for m, c, and k. Finally, the range parameters (a, k_2, and k_3) were found by fitting to the movable targets with all other parameters fixed. The calibration parameters for each wavelength are given in Table III.

The fit accuracy was assessed by applying the calibration parameters to an independent dataset of targets of known reflectance [again measured with an ASD Field Spec Pro spectroradiometer with contact probe (ASD inc., Boulder, CO, USA)]. This was a different calibration panel to those used to find the calibration parameters and was made by painting plywood with different mixtures of Humbrol matt white (34)

TABLE III
SALCA CALIBRATION PARAMETERS

Parameter	1545 nm	1063 nm
m	137.21	35.19
c	407.04	342.45
k	16.83	7.33
a	1.50	1.98
k_2	0.18	0.54
k_3	0.84	0.64

and black (33) paint. The laser power had to be calculated for each scan by fitting to the targets, and so the calibration could not be entirely independent, but any errors in the calibration would be apparent as a trend in the errors with reflectance or range. The SALCA retrieved reflectance had 5.6% RMSE and -1.9% bias for 1545 nm and 1.9% RMSE and $+0.02\%$ bias for 1063 nm. No trend with target reflectance or range was apparent, suggesting that the calibration was successful. This translated to a mean NDI bias of 0.027 and an RMSE of 0.055. For the leaf scans, laser power P_0 was calculated for each SALCA scan by fitting (4) to returns from the calibration panels in Fig. 3.

ACKNOWLEDGMENT

The authors would like to thank L. Schofield for collecting the data used in SALCA's calibration, J. Armston and Australia's Department of Science, Information Technology and Innovation for building the calibration panels, and the Terrestrial Laser Scanning International Interest Group, under the umbrella of which the calibration experiment took place (http://tlsiig.bu.edu/). They would also like to thank the former Newcastle University Botanic Gardens for providing the leaves used in this experiment and also the three anonymous reviewers for their helpful comments.

REFERENCES

[1] K. O. Niemann, G. Quinn, D. G. Goodenough, F. Visintini, and R. Loos, "Addressing the effects of canopy structure on the remote sensing of foliar chemistry of a 3-dimensional, radiometrically porous surface," *IEEE J. Select. Topics Appl. Earth Observ. Remote Sens.*, vol. 5, no. 2, pp. 584–593, Apr. 2012.

[2] D. J. Harding and C. C. Carabajal, "Icesat waveform measurements of within-footprint topographic relief and vegetation vertical structure," *Geophys. Res. Lett.*, vol. 32, no. 1, p. L21S10, Nov. 2005.

[3] J. Armston *et al.*, "Direct retrieval of canopy gap probability using airborne waveform lidar," *Remote Sens. Environ.*, vol. 134, pp. 24–38, Jul. 2013.

[4] K. Calders *et al.*, "Nondestructive estimates of above-ground biomass using terrestrial laser scanning," *Methods Ecol. Evol.*, vol. 6, no. 2, pp. 198–208, Feb. 2015.

[5] V. Wichmann, M. Bremer, J. Lindenberger, M. Rutzinger, C. Georges, and F. Petrini-Monteferri, "Evaluating the potential of multispectral airborne lidar for topographic mapping and land cover classification," *ISPRS Ann. Photogramm., Remote Sens. Spatial Inf. Sci.*, vol. 1, pp. 113–119, Sep./Oct. 2015.

[6] W. Y. Anthony, D. J. Harding, and P. W. Dabney, "Laser transmitter design and performance for the slope imaging multi-polarization photon-counting lidar (SIMPL) instrument," *Proc. SPIE*, p. 97260J, Mar. 2016.

[7] F. Morsdorf, C. Nichol, T. Malthus, and I. H. Woodhouse, "Assessing forest structural and physiological information content of multi-spectral LiDAR waveforms by radiative transfer modelling," *Remote Sens. Environ.*, vol. 113, no. 10, pp. 2152–2163, Oct. 2009.

[8] R. Gaulton, F. M. Danson, F. A. Ramirez, and O. Gunawan, "The potential of dual-wavelength laser scanning for estimating vegetation moisture content," *Remote Sens. Environ.*, vol. 132, pp. 32–39, May 2013.

[9] O. Nevalainen *et al.*, "Fast and nondestructive method for leaf level chlorophyll estimation using hyperspectral LiDAR," *Agricult. Forest Meteorol.*, vols. 198–199, pp. 250–258, Nov./Dec. 2014.

[10] J. M. Kestner *et al.*, "Goniometric observations of light scattered from soils and leaves," *Proc. SPIE*, vol. 0927, pp. 161–169, Jul. 1988.

[11] T. W. Brakke, J. A. Smith, and J. M. Harnden, "Bidirectional scattering of light from tree leaves," *Remote Sens. Environ.*, vol. 29, no. 2, pp. 175–183, Aug. 1989.

[12] X. Zhu, T. Wang, R. Darvishzadeh, A. K. Skidmore, and K. O. Niemann, "3D leaf water content mapping using terrestrial laser scanner backscatter intensity with radiometric correction," *ISPRS J. Photogramm. Remote Sens.*, vol. 110, pp. 14–23, Dec. 2015.

[13] J. U. Eitel, T. S. Magney, L. A. Vierling, and G. Dittmar, "Assessment of crop foliar nitrogen using a novel dual-wavelength laser system and implications for conducting laser-based plant physiology," *ISPRS J. Photogramm. Remote Sens.*, vol. 97, pp. 229–240, Nov. 2014.

[14] S. Kaasalainen, O. Nevalainen, T. Hakala, and K. Anttila, "Incidence angle dependency of leaf vegetation indices from hyperspectral lidar measurements," *Photogramm.-Fernerkundung-Geoinform.*, vol. 2016, no. 2, pp. 75–84, 2016.

[15] S. Shi, S. Song, W. Gong, L. Du, B. Zhu, and X. Huang, "Improving backscatter intensity calibration for multispectral LiDAR," *IEEE Geosci. Remote Sens. Lett.*, vol. 12, no. 7, pp. 1421–1425, Jul. 2015.

[16] S. Jacquemoud and S. L. Ustin, "Leaf optical properties: A state of the art," in *Proc. 8th Int. Symp. Phys. Meas. Signat. Remote Sens.*, Aussois, France, 2001, pp. 223–232.

[17] S. R. Sandmeier and A. H. Strahler, "BRDF laboratory measurements," *Remote Sens. Rev.*, vol. 18, nos. 2–4, pp. 481–502, 2000.

[18] H. Seeliger, "Theorie der beleuchtun staubformiger kosmishen masses insbesondere des saturinges," *Abhandl. Bayer. Akad. Wiss. Math-Nature. Kl. II*, vol. 18, pp. 1–72, 1893.

[19] W. A. Allen, "Transmission of isotropic light across a dielectric surface in two and three dimensions," *J. Opt. Soc. Amer.*, vol. 63, no. 6, pp. 664–666, 1973.

[20] F. M. Danson *et al.*, "Developing a dual-wavelength full-waveform terrestrial laser scanner to characterize forest canopy structure," *Agricult. Forest Meteorol.*, vols. 198–199, pp. 7–14, Nov./Dec. 2014.

[21] E. S. Douglas *et al.*, "Finding leaves in the forest: The dual-wavelength echidna Lidar," *IEEE Geosci. Remote Sens. Lett.*, vol. 12, no. 4, pp. 776–780, Apr. 2015.

[22] S. Fleming, A. Cottin, and I. H. Woodhouse, "The first spectral map of a forest understory from multispectral LiDAR," *Lidar News*, vol. 5, no. 1, pp. 26–30, 2015.

[23] M. Béland, J.-L. Widlowski, R. A. Fournier, J.-F. Côtéa, and M. M. Verstraete, "Estimating leaf area distribution in savanna trees from terrestrial LiDAR measurements," *Agricult. Forest Meteorol.*, vol. 151, no. 9, pp. 1252–1266, Sep. 2011.

[24] S. Hancock *et al.*, "Waveform lidar over vegetation: An evaluation of inversion methods for estimating return energy," *Remote Sens. Environ.*, vol. 164, pp. 208–224, Jul. 2015.

[25] S. Hancock *et al.*, "Characterising forest gap fraction with terrestrial lidar and photography: An examination of relative limitations," *Agricult. Forest Meteorol.*, vols. 189–190, pp. 105–114, Jun. 2014.

[26] B. Hosgood, S. Jacquemoud, G. Andreoli, J. Verdebout, G. Pedrini, and G. Schmuck, "Leaf optical properties experiment 93 (LOPEX93)," Eur. Comission-Joint Res. Centre, Ispra, Italy, Tech. Rep. EUR 16095 EN, 1994.

[27] L. A. Schofield, F. M. Danson, N. S. Entwistle, R. Gaulton, and S. Hancock, "Radiometric calibration of a dual-wavelength terrestrial laser scanner using neural networks," *Remote Sens. Lett.*, vol. 7, no. 4, pp. 299–308, 2016.

[28] Z. Li *et al.*, "Radiometric calibration of a dual-wavelength, full-waveform terrestrial lidar," *Sensors*, vol. 16, no. 3, p. 313, 2016.

[29] B. Garbow, K. Hillstrom, J. More, C. Markwardt, and S. Moshier. (Mar. 1980). *MPFIT: A MINPACK-1 Least Squares Fitting Library C*, Argonne National Laboratory. [Online]. Available: http://www.physics.wisc.edu/~craigm/idl/cmpfit.html

[30] B. Höfle and N. Pfeifer, "Correction of laser scanning intensity data: Data and model-driven approaches" *ISPRS J. Photo. Remot. Sens.*, vol. 62, no. 6, pp. 415–433, 2007.

Steven Hancock, photograph and biography not available at the time of publication.

Rachel Gaulton, photograph and biography not available at the time of publication.

F. Mark Danson, photograph and biography not available at the time of publication.